COBEM 2023 27TH INTERNATIONAL CONGRESS OF MECHANICAL ENGENEERING

ABCM Brazilian Society of Mechanical Sciences and Engineering
27th ABCM International Congress of Mechanical Engineering
December 04-08, 2023, Florianópolis-SC, Brazil

COB-2023-1734
IDENTIFICATION OF MODAL PARAMETERS OF COUPLED ROTOR FOUNDATION SYSTEM VIA AUTOMATIC OPERATIONAL MODAL ANALYSIS

Nathali Dreher
Tiago Machado
School of Mechanical Engineering, University of Campinas (UNICAMP), 200 Mendeleyev street, Campinas, SP 13083-860, Brazil
n265296@dac.unicamp.br
tiagomh@fem.unicamp.br

Thomas Paulsen
Ilmar Santos
Department of Civil and Mechanical Engineering, Technical University of Denmark (DTU), Koppels Allé 404, 2800 Kgs. Lyngby, Denmark
ththpa@dtu.dk
ilsa@dtu.dk

Abstract. *Operational Modal Analysis (OMA) extracts modal parameters of systems that are excited by unknown ambiental excitation, being broadly used in the monitoring of civil structures. In the past decades, research has been made to enable the application of OMA in rotating machines, dealing with challenges such as harmonic excitation, nonlinearities, and the lack of proper excitation. With the popularization of machine learning techniques, many researchers have been using these tools to overcome some challenges in this research field. Clustering techniques, that can group information about datasets without prior knowledge of their characteristics, has been used along with statistical methods to automate OMA so that it can be used for condition monitoring. Recently, automatic OMA (AOMA) was applied to rotating machinery data. This paper evaluates one of these AOMA algorithms, successfully tested with data from a test rig with a rotor supported by hydrodynamic bearings, in a more complex dataset, with data from a rotor supported by magnetic bearings and influenced by gas seal. The results show that the proposed algorithm can extract modal parameters close to the ones extracted by EMA and by the mathematical modelling of the test rig, being robust even when a more complex system is analyzed.*

Keywords: *Operational Modal Analysis, Rotating Machinery, Machine Learning, System Identification*

1. INTRODUCTION

Vibration patterns of structures, machines, and vehicles are described by the modal parameters of the system. Changes in these parameters indicate that the system has been altered in some way, a possible indication of faults or failures. Therefore, extracting and monitoring the system's modal parameters is a matter of interest in the context of condition and health monitoring. Generally, the modal parameters are computed through mathematical modeling and extracted through Experimental Modal Analysis (EMA) tests in the existing system, which requires knowledge of the dynamic behavior of the system, and known and controllable excitation sources, respectively. Operational Modal Analysis (OMA) has been an important topic of research in the past decades because it enables modal parameter extraction without the need of known excitation sources and keeping the system on operation for testing. OMA considers that the excitation found during the system's operation is white noise with a broad frequency range that is capable of exciting all modes of interest. Moreover, it assumes that the system is linear and time invariant. OMA has been widely used for the modal analysis of civil structures because they usually can be considered linear and time invariant and they are subjected to similar white noise excitation.

The application of OMA in rotating machines is a topic of growing interest especially because of its advantages. However, rotating machines are subjected to complex load conditions and are themselves more complex than civil structures, requiring additional data processing to accurately extract the modal parameters of interest. Some solutions to these challenges have already been studied, such as the application of OMA in non-linear or time-varying systems (Vesterholm et al., 2019; Kang and Zeng, 2023), in systems that are subjected to harmonic excitation (Brandt, 2019; Gioia et al., 2019; Peeters et al., 2019; Gres et al., 2021; Xu et al., 2023), and in rotating systems with closely spaced forward and backward modes (Dreher et al., 2022).

Another topic of interest in the context of OMA and condition and health monitoring is the Automatic OMA (AOMA). Although OMA is more versatile than traditional EMA, the results' analysis is still highly dependent on a

qualified professional. Therefore, several algorithms that combine statistical and machine learning techniques with OMA techniques have been proposed in the last few decades to fully automate OMA. Some classical research on the subject are the works of Magalhães et al. (2009) and Reynders et al. (2012). More recently, Priou et al. (2022) proposed an algorithm to automatically extract modal parameters considering the modes' uncertainties, validating the algorithm on vibration data from two bridges. Mugnaini et al. (2022) proposed a fully automated approach, successfully applying it to a numerical case study and to data from an Airbus H135 helicopter blade. Shu et al. (2023) developed a multi-task deep neural network that can automatically extract independent modes from multi-mode vibration responses of structures, further determining the modal parameters with conventional random decrement technique (RDT) and curve fitting approach. Once the network is trained, there is no need to manually set thresholds or indexes. When applied to data from a spring-mass-damper model and a long-span cable-stayed bridge, the proposed neural network achieved high accuracy and computational efficiency. Volkmar et al. (2023) presented a fully automated modal analysis approach that learns optimal parameters on a supervised manner based on a single manual modal analysis and choses new parameters with statistical methods. The approach was evaluated in ground vibration test data (EMA) and flight vibration data (OMA), showing good accuracy and computational efficiency. Zhong et al. (2023) proposed an AOMA method that uses an adaptive clustering method based on DBSCAN clustering with automatic selection of parameters. The method's performance was investigated via numerical analyses and the measured data from an actual bridge, being able to identify the modal parameters under various scenarios, with low bias and variance.

All research mentioned so far were developed for and tested with bridges and other simple models and structures. However, AOMA algorithms that focus on extracting modal parameters of coupled rotor foundation systems were already proposed by Paulsen et al. (2023) and Dreher et al. (2023). Paulsen et al. (2023) developed an AOMA algorithm to extract modal parameters for a bed plate of a rotor-foundation system when the rotor is affected by active magnetic bearings and gas seals. Dreher et al. (2023) proposed an AOMA method to extract the rotor's modal parameters, validating it in vibration signals from a test rig supported by hydrodynamic bearings and rolling bearings. It is important to highlight that both papers worked with rotating machinery parts, which is not common in the context of OMA because of the abovementioned challenges. To investigate the robustness of the algorithm proposed by Dreher et al. (2023), this paper applies the algorithm on the data collected and analyzed by Paulsen et al. (2023), that comes from a more complex system and has mainly modal parameters from the foundation. The algorithm from Dreher et al. (2023) is briefly presented in section 2.1 and the dataset from Paulsen et al. (2023) is presented in section 2.2. The results are analyzed in terms of the stabilization diagrams obtained with the Stochastic Subspace Identification (SSI) method and the extracted modal parameters, which are compared with EMA modal parameters from the foundation, that supports the rotor and is influenced by it, and OMA results from Paulsen et al. (2023), as presented in section 3. Focus is given to the modal analysis of a non-rotating structure that supports the rotor rather than the rotor itself.

2. METHODOLOGY

2.1 AOMA algorithm

The algorithm proposed by Dreher et al. (2023) can be summarized into the following steps:

1. Create the stabilization diagram using the SSI algorithm and classify each pole based on stabilization criteria,
2. Clear the stabilization diagram using the Hard Validation Criteria (HVC),
3. Group stable poles that represent the same mode using agglomerative hierarchical clustering,
4. Remove from each cluster poles of repeated orders, so that only one pole of this order remains,
5. Eliminate small clusters that probably represent clusters of spurious or mathematical poles,
6. Perform an outlier detection based on the boxplot method,
7. Describe the global modes by the clusters mean frequency, mean damping, and mean mode shape,
8. Group poles with mode shapes of high correlation using agglomerative hierarchical clustering.

In order to support the results' analysis presented in section 3, it is important to further explain the characteristics of the stabilization diagram and the final result of the algorithm.

The stabilization diagram is build performing the SSI with increasing model orders and plotting the natural frequency of the resulting poles in the x axis and the order in which they were extracted in the y axis. All poles are inspected and classified according to the following evaluation. A k-order pole is stable if there is at least one pole in the $(k-1)$-order that satisfies the following stabilization criteria from one order to the other: frequency variation limit, damping ratio variation limit, and Moral Assurance Criterion (MAC) limit. All poles that fulfill the stabilization criteria are classified as stable, and all that do not are classified as not stable, in accordance with the algorithm's first step. This is important because physical modes of the system can be identified by the alignment of stable poles along different model orders.

In sequence, each pole (stable and not stable) is analyzed to verify if it respects the Hard Validation Criteria (HVC). The idea behind the HVC is to remove all certainly spurious poles from the following steps, that is, poles with negative damping ratio and no complex conjugated pair. Moreover, performing initial tests allow the analyst to know the normal

behavior of the system, including the normal range of damping ratios. Thus, poles with damping ratios out of this range are also considered spurious. In that way, the stabilization diagram presents stable, not stable, and spurious poles. Only stable poles are considered for the following steps of the algorithm.

The hierarchical clustering is then employed to group poles that characterize the same physical modes. The following steps are used to remove spurious or inaccurate poles that were not excluded by the stabilization criteria or the HVC, making the results more accurate. The algorithm concludes taking mean frequencies, mean damping ratios, and mean mode shapes of each group of poles to represent each global mode.

2.2 Dataset's description

The test rig employed by Paulsen et al. (2023) is displayed on Figure 1, being composed of an electric motor connected to a drive shaft through a belt drive. The drive shaft controls the main rotor through a flexible coupling. The main rotor is levitated in the lateral directions by active magnetic bearings and influenced by two smooth annular seals mounted in a back-to-back configuration. The modules carrying the motor, drive shaft, active magnetic bearings, and seal geometries are placed on a bed plate. The authors focused the investigation on the identification of vibration patterns present in the bed plate when the seal inlet pressure changes.

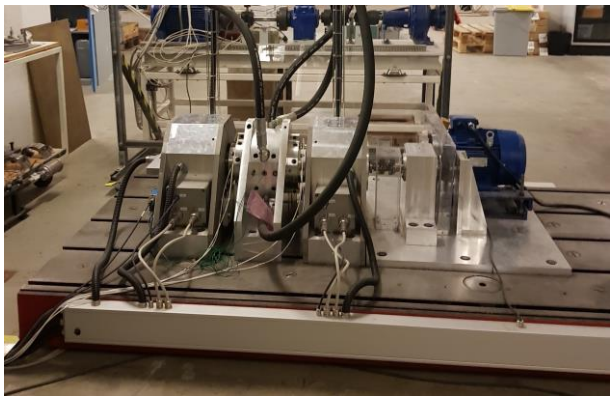

Figure 1. Test rig of a rotor supported by active magnetic bearings and influenced by gas seal.

EMA tests were performed using an excitation hammer to obtain estimates of the modal parameters of the system during three operating conditions, seal inlet pressures of 0 bar, 1.3 bar and 2.7 bar. The modal parameters for each operating condition were also estimated with a mathematical model of the test rig. Further details about the EMA tests and the mathematical model can be found in Paulsen et al. (2023).

Data for OMA tests, on the other hand, were collected for five operating conditions, pressures of 0 bar and white noise excitation, 1.3 bar and no excitation, 1.3 bar and white noise excitation, 2.7 bar and no excitation, and 2.7 bar and white noise excitation. The authors' idea was to evaluate whether the seal forces could be used as white noise excitation for OMA, which was proved possible. For OMA, data was collected with one stationary accelerometer and one roving accelerometer, that was placed in 13 different positions of the bed plate, as presented in Figure 2. For all 5 conditions of OMA tests, 13 measurements were collected with both accelerometers, the stationary and roving ones, during 128s and with sampling frequency of 3012 Hz.

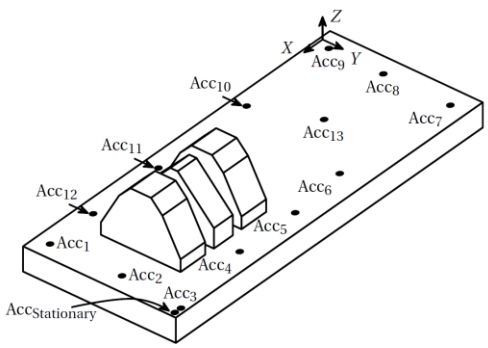

Figure 2. Test rig with the 13 positions of the roving accelerometer.

Summarizing the available data for OMA, tests with the following conditions are available for each of the 13 configurations:

1. 0 bar pressure and white noise excitation,
2. 1.3 bar pressure and no excitation,
3. 1.3 bar pressure and white noise excitation,
4. 2.7 bar pressure and no excitation,
5. 2.7 bar pressure and white noise excitation.

3. RESULTS

In this section, the results of the application of the algorithm presented by Dreher et al. (2023) in the data collected by Paulsen et al. (2023) are discussed. Since the AOMA algorithm depends on the results of the SSI algorithm, the parameters of this algorithm need to be selected, which is presented in section 3.1. Then, the AOMA algorithm's robustness is proved in section 3.2, varying the AOMA's parameters and comparing the results with the ones obtained in Paulsen et al. (2023) from EMA and OMA analysis.

3.1 Stabilization Diagram analysis

The quality of the stabilization diagram generated by the SSI algorithm is based on the right selection of the number of block rows in the Hankel matrix (i), the method (Unweighted Principal Component – UPC, Principal Component – PC, and Canonic Variate Algorithm – CVA) of the data driven SSI (SSI-DATA), and the maximum order of the model. These parameters are dependent on the systems' characteristics and are selected by experienced users from case to case.

For the dataset employed in Dreher et al. (2023), the selected number of block rows was 100, the SSI-DATA method was the UPC, and the maximum order was 100. In Paulsen et al. (2023), the authors found the ideal number of block rows as 256 (2^8) and employed the covariance driven SSI (SSI-COV) with maximum order of 128 (2^7). In order to define the best parameters for this dataset using the algorithm from Dreher et al. (2023), the stabilization diagrams generated with different parameters were visually analyzed. The stabilization diagrams are used because the choice of these parameters directly affect the diagrams' quality.

The stabilization diagrams in Figure 3 were generated with measurements from condition 1 (0 bar and white noise excitation) and roving sensor 6, using 100 (a) and 256 (b) block rows. The SSI results are presented as circles (poles) that indicate the natural frequency in Hz (x axis) and the model order (y axis) of each possibly physical mode of the system. Each pole is identified as stable (red), not stable (green), and spurious (blue) in accordance with the natural frequency, damping ratio, and mode shape. The presence of a physical mode is indicated by the alignment of stable poles, and the presence of a mathematical mode or a harmonic frequency exciting the system is indicated by not stable or spurious poles. The curves in the background are the results from the Frequency Domain Decomposition (FDD) method. From the results, one can see that the diagram generated with 256 block rows has a higher number of stable poles and better-defined alignments of stable poles, being better for modal parameter identification. The stabilization diagrams of different conditions and sensors were also analyzed, and the results were similar.

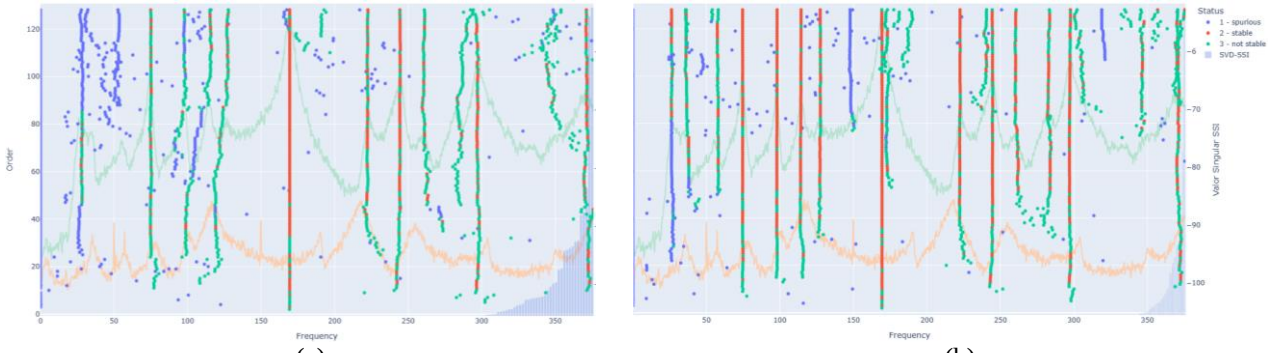

(a) (b)

Figure 3. Stabilization diagrams from condition 1 and roving sensor 6 with $i = 100$ (a) and $i = 256$ (b).

The higher the number of block rows, the higher is the computational cost. Considering that the results with 256 block rows were good for modal identification and the number is the same found as ideal in Paulsen et al. (2023), it will be selected as the ideal number of block rows for this case. Still, an increase of 17% in the number of block rows was tested, from 256 (Figure 4-a) to 300 (Figure 4-b) for the measurement from condition 5 and roving sensor 6. From the results of the stable poles, displayed in Figure 4, one can see that the increase in the number of block rows slightly increased the number of stable poles near the frequency of 120 Hz, which has a physical mode of interest. However, the stability of the other frequency ranges of interest didn't change significantly. Moreover, the FDD results indicates that the main reason

for the weak visualization of the frequency of 120 Hz is the small number of sensors or the weak excitation of this mode, and not the SSI method or parameters.

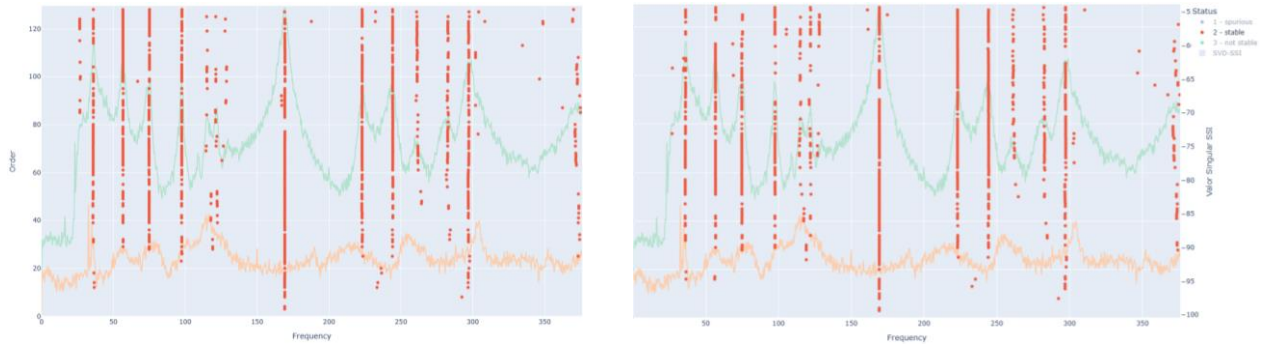

(a) (b)

Figure 4. Stabilization diagrams from condition 5 and roving sensor 6 with $i = 256$ (a) and $i = 300$ (b).

The influence of the maximum model order was also evaluated. Stabilization diagrams with maximum orders of 128 and 256 were compared for both $i = 128$ and $i = 256$. From the results, it was concluded that the increase in the number of block rows still provide more stable poles than the increase in the order. And the increase in both parameters (order and number of block rows) leads to an enormous number of probably spurious poles that were not identified as such with HVC. This happens because the SSI algorithm attempts to fit the data precisely. The higher the model order, the more modes are used for fitting. Therefore, the algorithm results in fitting noise and other characteristics of the vibration signal that are not related to the dynamics of the system.

The stabilization diagrams were generated with all SSI-DATA methods, UPC, PC, and CVA. From a visual inspection of all diagrams, the results with UPC and PC methods were very similar, but there is a slight improvement in the poles' stability using the PC method. Comparing the PC and the CVA methods, the poles stability is improved only on the higher orders of the CVA method. The damping ratios are slightly affected by the change, however, even with the EMA's expected results, it is impossible to tell if these changes are an improvement or not. Moreover, the CVA method increases the number of spurious poles. Therefore, the chosen method is the PC.

For the following analysis, the selected number of block rows is 256, the SSI-DATA method is the PC, and the maximum order is 128.

3.2 Modal parameter analysis

All results presented so far were compared in terms of the stabilization diagram. To verify how the limits of stabilization and damping ratio and the hierarchical clustering threshold influence the AOMA algorithm, the results will be compared in terms of the extracted global modes. The global modes are analyzed because the choice of these parameters doesn't affect the poles alignment in the stabilization diagram, only their classification. Since there are 13 measurements (13 positions for the roving sensor) for each operating condition, 13 modal analysis results are obtained for each condition. In order to compare these results with the ones presented in Paulsen et al. (2023), similar global modes within a single operating condition were grouped together in terms of mean value, which provided a single group of modal parameters for each condition. Therefore, each change in the SSI or AOMA parameters will be evaluated in terms of the mean modal parameters extracted with these changes.

In Dreher et al. (2023), the damping ratio limit was chosen as 0.3% to 10%, the frequency variation limit as 0.2%, the damping ratio variation limit as 2%, the minimum MAC value as 95%, and the threshold value for the hierarchical clustering as 0.01. The same parameters were used to process the dataset from Paulsen et al. (2023). The results are displayed in Table 1 to Table 3, along with the EMA and OMA results from Paulsen et al. (2023). From the overview, one can see that the results obtained with my AOMA algorithm from Dreher et al. (2023) are similar to the EMA reference and to the results obtained by Paulsen et al. (2023), that were validated through the EMA reference and the mathematical model of the test rig. There are only a few modes that are identified by one algorithm and not the other, or that are identified with different damping ratios when compared to the EMA reference. For most modes that the present algorithm is unable to identify or identifies with significant deviation from the reference, the problem can be traced back to the stabilization diagram, not the algorithm's ability to automatically interpret the stabilization diagram. It is important to highlight that the AOMA parameters are the same configurated for the test rig with a rotor supported by a hydrodynamic bearing, that is simpler than the one from Paulsen et al. (2023). This means that even for the more complex case, the AOMA algorithm from Dreher et al. (2023) was able to identify most physical modes of interest with high accuracy compared to EMA and to the mathematical model. This indicates the robustness of the AOMA algorithm.

Table 1. Results with original parameters from Dreher et al. (2023) for condition with 0 bar pressure and white noise.

EMA		**OMA (Paulsen et al., 2023)**		**OMA (Dreher et al., 2023)**	
ω_n [Hz]	ζ [%]	ω_n [Hz]	ζ [%]	ω_n [Hz]	ζ [%]
25.64	8.67	25.84	5.50	26.27	8.84
34.90	3.59	35.62	3.73	35.46	3.15
44.24	14.81	-	-	-	-
56.34	2.31	55.32	3.00	54.58	2.59
74.09	2.05	74.61	1.55	74.51	1.37
95.93	0.98	98.10	0.97	98.07	0.97
114.30	1.96	114.02	1.63	114.30	1.67
120.16	3.04	127.02	1.58	127.33	2.39
169.43	0.72	169.01	1.20	169.41	1.09
190.46	0.90	186.01	1.18	-	-

Table 2. Results with original parameters from Dreher et al. (2023) for conditions with 1.3 bar pressure.

EMA		**OMA (Paulsen et al., 2023) No excitation**		**OMA (Dreher et al., 2023) No excitation**		**OMA (Paulsen et al., 2023) White noise**		**OMA (Dreher et al., 2023) White noise**	
ω_n [Hz]	ζ [%]	ω_n [Hz]	ζ [%]	ω_n [Hz]	ζ [%]	ω_n [Hz]	ζ [%]	ω_n [Hz]	ζ [%]
24.73	8.69	25.81	2.27	26.46	4.31	26.03	4.69	26.37	8.24
34.71	4.00	35.42	3.19	34.07	1.48	32.44	4.96	36.00	3.79
42.84	13.02	-	-	-	-	36.13	3.93	-	-
55.94	2.08	57.10	1.04	56.93	1.86	56.39	5.67	56.40	3.04
73.99	1.91	74.41	1.32	74.55	1.57	74.51	1.38	74.53	1.38
95.10	1.55	98.60	0.85	98.65	1.06	98.20	0.91	98.13	0.90
114.18	1.56	114.02	1.63	114.61	1.83	115.01	1.52	114.47	1.49
121.34	2.83	-	-	-	-	127.02	1.85	127.58	2.23
-	-	157.00	0.60	-	-	-	-	-	-
169.40	0.82	169.01	1.19	169.43	1.20	169.01	1.13	169.37	1.10
-	-	177.01	1.18	-	-	-	-	-	-
190.29	1.02	-	-	190.98	0.88	183.01	0.81	-	-

Table 3. Results with original parameters from Dreher et al. (2023) for conditions with 2.7 bar pressure.

EMA		**OMA (Paulsen et al., 2023) No excitation**		**OMA (Dreher et al., 2023) No excitation**		**OMA (Paulsen et al., 2023) White noise**		**OMA (Dreher et al., 2023) White noise**	
ω_n [Hz]	ζ [%]	ω_n [Hz]	ζ [%]	ω_n [Hz]	ζ [%]	ω_n [Hz]	ζ [%]	ω_n [Hz]	ζ [%]
25.25	9.53	26.63	4.39	25.79	4.96	26.15	5.93	26.47	7.86
34.91	2.88	35.35	5.54	35.46	2.29	36.21	2.87	35.87	3.35
48.46	9.30	-	-	40.27	1.53	40.30	6.92	42.63	8.10
55.79	1.92	56.71	1.92	56.84	2.55	56.54	3.73	57.04	3.44
74.07	1.77	75.01	1.92	74.78	2.37	73.91	1.69	74.90	1.95
95.61	2.52	98.20	0.82	98.39	0.86	97.70	0.97	97.63	0.90
114.44	2.42	115.02	1.89	115.19	1.59	115.01	1.50	115.00	1.30
120.91	4.36	-	-	-	-	-	-	121.63	1.32
-	-	-	-	-	-	139.04	2.34	129.11	2.33
169.16	0.87	169.01	1.25	169.49	1.26	169.01	1.15	169.32	1.18
191.63	1.42	-	-	191.04	0.81	-	-	-	-

One can see that the damping ratio of the first mode (around 25 Hz and 9% damping) is difficult to estimate via OMA, and the estimations are usually lower than the reference. Taking a closer look to Table 1 to Table 3, there are also physical modes extracted by EMA with damping ratio above 10% (around 45 Hz and 13% damping), values above the damping ratio limit employed for AOMA. Therefore, another set of AOMA results was generated using the damping ratio limit of 15%. The results for the modes of interest are displayed in Table 4, from which one can see that the change in the damping ratio limit improved some of the extracted damping ratios (see conditions 1 and 2). But OMA is still unable to identify some modes of interest around 42 Hz.

Table 4. Results with damping ratio limit of 15% for all conditions.

Condition	EMA		OMA - Original parameters		OMA - Damping ratio limit of 15%	
	ω_n [Hz]	ζ [%]	ω_n [Hz]	ζ [%]	ω_n [Hz]	ζ [%]
1	25.64	8.67	25.80	5.50	26.36	10
	44.24	14.81	-	-	-	-
2	24.73	8.69	26.46	4.31	27.05	5.91
	42.84	13.02	-	-	-	-
3	24.73	8.69	26.37	8.24	26.46	9.29
	42.84	13.02	-	-	-	-
4	25.25	9.53	25.79	4.96	25.79	4.96
	48.46	9.30	40.27	1.53	40.27	1.53
5	25.25	9.53	26.47	7.86	26.52	8.10
	48.46	9.30	42.63	8.10	42.55	8.79

To verify if the results can be further improved, identifying more physical modes of interest or modal parameters with higher accuracy, the following changes will also be adopted: frequency variation limit of 0.5% (2.5x the original), damping variation limit of 4% (2x the original), MAC limit of 90% (5% lower than the original). It is important to highlight that the changes are all in the sense of making the stabilization criteria wider, enabling the classification of more poles as stable and, therefore, providing more poles for the AOMA method to process. The results of these changes are displayed on Table 5 to Table 7. For condition 0 (Table 5), one can see that the changes enabled the identification of one more physical mode of interest, around 190 Hz, and didn't alter the other results, that were already close to the EMA reference. For condition 2 (Table 6), the mode of 34.68 Hz was identified with a damping ratio closer to the reference. For conditions 3 (Table 6), the mode of 56 Hz was split into two. Evaluating the stabilization diagrams, one can verify that a single strong alignment of stable poles around that frequency is split into two at higher orders. Since using greater limits for the stabilization diagram enables a wider frequency range of poles around this mode to be identified as stable, these two alignments were identified by the AOMA algorithm. Further investigations are needed to verify if there are two closely spaced modes around this frequency or if these two alignments appear as an attempt of the SSI method to fit the data. All other modes of these conditions were similar to the ones extracted using the original stabilization parameters. For conditions 4 (Table 7), the results were similar to the ones extracted using the original stabilization parameters and to the EMA reference. Finally, for condition 5 (Table 7) there are several physical modes of interest that were split into two, results that can also be traced back to the stabilization diagram's result. Apart from the two modes near 56 Hz, the duplications are caused because there is not a strong stabilization around the frequencies of interest.

Table 5. Results with new parameters for condition with 0 bar pressure and white noise.

EMA		OMA - Original parameters		OMA - New parameters	
ω_n [Hz]	ζ [%]	ω_n [Hz]	ζ [%]	ω_n [Hz]	ζ [%]
25.64	8.67	26.27	8.84	26.32	9.07
34.90	3.59	35.46	3.15	35.55	3.40
44.24	14.81	-	-	-	-
56.34	2.31	54.58	2.59	56.15	3.35
74.09	2.05	74.51	1.37	74.51	1.37
95.93	0.98	98.07	0.97	98.06	0.97
114.30	1.96	114.30	1.67	114.29	1.66
120.16	3.04	127.33	2.39	127.35	2.45
169.43	0.72	169.41	1.09	169.40	1.09
190.46	0.90	-	-	190.18	0.76

Table 6. Results with new parameters for conditions with 1.3 bar pressure.

EMA		**OMA - No excitation Original parameters**		**OMA - No excitation New parameters**		**OMA - White noise Original parameters**		**OMA - White noise New parameters**	
$\omega_n\ [Hz]$	ζ [%]	$\omega_n\ [Hz]$	ζ [%]	$\omega_n\ [Hz]$	ζ [%]	$\omega_n\ [Hz]$	ζ [%]	$\omega_n\ [Hz]$	ζ [%]
24.73	8.69	26.46	4.31	26.57	4.59	26.37	8.24	26.35	8.29
34.71	4.00	34.07	1.48	34.37	3.54	36.00	3.79	35.90	3.90
42.84	13.02	-	-	-	-	-	-	-	-
-	-	-	-	-	-	-	-	55.54	3.41
55.94	2.08	56.93	1.86	56.94	1.96	56.40	3.04	56.54	3.02
73.99	1.91	74.55	1.57	74.54	1.59	74.53	1.38	74.53	1.38
95.10	1.55	98.65	1.06	98.66	1.07	98.13	0.90	98.13	0.89
114.18	1.56	114.61	1.83	114.61	1.84	114.47	1.49	114.47	1.50
121.34	2.83	-	-	-	-	127.58	2.23	127.58	2.21
169.40	0.82	169.43	1.20	169.43	1.20	169.37	1.10	169.37	1.10
190.29	1.02	190.98	0.88	190.52	0.75	-	-	-	-

Table 7. Results with new parameters for conditions with 2.7 bar pressure.

EMA		**OMA - No excitation Original parameters**		**OMA - No excitation New parameters**		**OMA - White noise Original parameters**		**OMA - White noise New parameters**	
$\omega_n\ [Hz]$	ζ [%]	$\omega_n\ [Hz]$	ζ [%]	$\omega_n\ [Hz]$	ζ [%]	$\omega_n\ [Hz]$	ζ [%]	$\omega_n\ [Hz]$	ζ [%]
25.25	9.53	25.79	4.96	25.45	4.82	26.47	7.86	26.62	8.04
34.91	2.88	35.46	2.29	35.56	2.25	35.87	3.35	34.60	4.15
-	-	-	-	-	-	-	-	36.08	3.25
48.46	9.30	40.27	1.53	40.17	1.60	42.63	8.10	42.61	8.04
55.79	1.92	56.84	2.55	56.87	2.77	57.04	3.44	56.75	3.37
-	-	-	-	-	-	-	-	57.71	3.63
-	-	-	-	-	-	-	-	73.84	2.56
74.07	1.77	74.78	2.37	74.78	2.38	74.90	1.95	74.91	1.95
95.61	2.52	98.39	0.86	98.29	0.82	97.63	0.90	97.63	0.90
114.44	2.42	115.19	1.59	115.19	1.59	115.00	1.30	115.08	1.35
120.91	4.36	-	-	-	-	121.63	1.32	121.65	1.15
-	-	-	-	-	-	129.11	2.33	128.42	2.32
-	-	-	-	-	-	-	-	163.87	0.88
169.16	0.87	169.49	1.26	169.49	1.27	169.32	1.18	169.32	1.18
191.63	1.42	191.04	0.81	190.85	1.02	-	-	-	-

The threshold limit of the hierarchical clustering was set to 0.013 (the original value was 0.01), so that more poles could be clustered in the same group. With this change, most modes that were divided into two groups in Table 7 were merged back to a single group. Moreover, further steps can be implemented to evaluate if these groups with close mean frequencies are groups of the same physical mode, as done by Paulsen et al. (2023), and, if so, either group them together or choose one of them as more accurate.

Even with changes in the AOMA parameters, it was not possible to identify all modes of interest for all conditions. Physical modes of 40Hz, 127Hz, and 190Hz presented weak stabilization in the stabilization diagrams of most conditions, which explain their absence in the results. Thus, they would likely not be identified as physical modes of the system by an experienced analyst and could not be identified by the AOMA algorithm. Some extra modes, that were not identified in EMA tests, were identified by the AOMA algorithms from Paulsen et al. (2023) and Dreher et al. (2023). Evaluating the stabilization diagrams, one can see a strong alignment of these modes (129Hz and 164Hz), that look like true physical modes present in the measurements. These findings indicate that the AOMA algorithm could properly interpret the stabilization diagrams.

4. CONCLUSIONS

In this paper the Automatic Operational Modal Analysis (AOMA) algorithm proposed by Dreher et al. (2023) and tested in a test rig with a rotor supported by hydrodynamic bearings was evaluated. The algorithm was applied to a more complex dataset, with a rotor supported by active magnetic bearings and influenced by gas seal pressure. The SSI parameters were adjusted for the new dataset, which is a common practice since their values vary from system to system. The parameters of the AOMA algorithm were also adjusted, and the results demonstrated that even for a more complex rotating system, the original parameters could accurately extract the majority of the physical modes of interest, that are

related to the foundation that supports the rotor and is influenced by it. Only small changes in the parameters were made to slightly improve the results. The modes that were not identified by the AOMA method were weakly excited modes, with weak stabilization in the diagrams, and it is likely that an experienced analyst wouldn't classify these modes as physical modes of the system. Finally, from these results, one can see that the AOMA algorithm from Dreher et al. (2023) is good for extracting modal parameters from systems that are composed of a foundation supporting a rotating machine, which validates its robustness.

5. ACKNOWLEDGEMENTS

The authors would like to thank CAPES, Coordination for the Improvement of Higher Education Personnel, and PRPG, Pro-Rectory of Graduate Studies at UNICAMP, for the financial support, and the Department of Civil and Mechanical Engineering from Technical University of Denmark for the support that made this work possible.

6. REFERENCES

Brandt, A., 2019. "A signal processing framework for operational modal analysis in time and frequency domain". *Mechanical Systems and Signal Processing.* Vol. 115, p. 380-393. https://doi.org/10.1016/j.ymssp.2018.06.009.

Dreher, N.R., Storti, G.C. and Machado, T.H., 2022. "Directional coordinates for the identification of backward and forward frequencies of rotating machines via OMA". In *Proceedings of the 9th International Operational Modal Analysis Conference – IOMAC 2022*. Vancouver, Canada.

Dreher, N.R., Storti, G.C. and Machado, T.H., 2023. "Automated Operational Modal Analysis for Rotating Machinery Based on Clustering Techniques". *Sensors*. Vol. 23, p. 1665. https://doi.org/10.3390/s23031665.

Gioia, N., Daems, P.J., Peeters, C., El-Kafafy, M., Guillaume, P. and Helsen, J., 2019, "Influence of the Harmonics on the Modal Behavior of Wind Turbine Drivetrains". *Rotating Machinery, Vibro-Acoustics & Laser Vibrometry*. Vol. 7, p. 231-238, 2019. https://doi.org/10.1007/978-3-319-74693-7_22.

Gres, S., Döhler, M., Andersen, P. and Mevel, L., 2021. "Kalman filter-based subspace identification for operational modal analysis under unmeasured periodic excitation". *Mechanical Systems and Signal Processing.* Vol. 146. https://doi.org/10.1016/j.ymssp.2020.106996.

Kang, J. and Zeng, S., 2023. "Uncertainty quantification in operational modal analysis of time-varying structures based on time-dependent autoregressive moving average model". *Journal of Sound and Vibration*, Vol. 548, p. 117549. https://doi.org/10.1016/j.jsv.2022.117549.

Magalhães, F., Cunha, A. and Caetano, E., 2009. "Online automatic identification of the modal parameters of a long span arch bridge". *Mechanical Systems and Signal Processing*. Vol. 23, n. 2, p. 316-329. https://doi.org/10.1016/j.ymssp.2008.05.003.

Mugnaini, V., Fragonara L.Z. and Civera, M., 2022. "A machine learning approach for automatic operational modal analysis". *Mechanical Systems and Signal Processing*. Vol. 170, p. 108813. https://doi.org/10.1016/j.ymssp.2022.108813.

Paulsen, T.T., Damsgaard, S.V., Clemmensen, L.K.H. and Santos, I.F., 2023. "Automated Modal Parameter Estimation for Coupled Rotor-Foundation Systems Using Seal Forces as Excitation Source". *SSRN Elsevier*. https://dx.doi.org/10.2139/ssrn.4377087

Peeters, C., Gioia, N., Helsen, J. and Guillaume, P., 2019. "Identification of Noise Vibration and Harshness Behavior of Wind Turbine Drivetrain under different operating conditions". *Energies*. Vol. 12, n. 17:3401. https://doi.org/10.3390/en12173401.

Priou, J., Gres, S., Perrault, M., Guerineau, L. and Döhler, M., 2022. "Automated uncertainty-based extraction of modal parameters from stabilization diagrams". In *Proceedings of the 9th International Operational Modal Analysis Conference – IOMAC 2022*. Vancouver, Canada.

Reynders, E., Houbrechts, J. and De Roeck, G., 2012. "Fully automated (operational) modal analysis". *Mechanical Systems and Signal Processing*. Vol. 29, p. 228-250. https://doi.org/10.1016/j.ymssp.2012.01.007.

Shu, J., Zhang, C., Gao, Y. and Niu, Y., 2023. "A multi-task learning-based automatic blind identification procedure for operational modal analysis". Vol. 187, p. 109959. https://doi.org/10.1016/j.ymssp.2022.109959.

Vesterholm, K. K., Brincker, R. and Brandt, A.B., 2019. "Detection of nonlinear behavior using the Random Decrement Technique". In *Proceedings of the 8th International Operational Modal Analysis Conference - IOMAC 2019*. Copenhagen, Denmark.

Volkmar, R., Soal, K., Govers, Y. and Böswald, M., 2023. "Experimental and operational modal analysis: Automated system identification for safety-critical applications". *Mechanical Systems and Signal Processing*. Vol. 183, p. 109658. https://doi.org/10.1016/j.ymssp.2022.109658.

Xu, M., Au, F.T.K., Wang, S. and Tian, H., 2023. "Uncertainty quantification in operational modal analysis of time-varying structures based on time-dependent autoregressive moving average model". *Journal of Sound and Vibration*, Vol. 545, p. 117436. https://doi.org/10.1016/j.jsv.2022.117436.

Zhong, Q.M., Chen, S.Z., Sun, Z. and Tian, L.C., 2023. “Fully automatic operational modal analysis method based on statistical rule enhanced adaptive clustering method”. *Engineering Structures*. Vol. 274, p. 115216. https://doi.org/10.1016/j.engstruct.2022.115216.

7. RESPONSIBILITY NOTICE

The authors are the only responsible for the printed material included in this paper.